14th International Symposium on Turbulence and Shear Flow Phenomena (TSFP14)
Heidelberg, Germany, July 28–31, 2026

THE DRAG FORCE ON A DECELERATING ROUND PLATE

Nicola Savelli, Ali R Khojasteh & Jerry Westerweel*
Laboratory for Aero & Hydrodynamics
Delft University of Technology
Mekelweg 2, 2628 CD Delft, The Netherlands
j.westerweel@tudelft.nl

ABSTRACT

We present experimental results on the drag force on a decelerating disk. We use a gantry robot to precisely control the motion of a disk in a large water-filled tank. The initial state is stationary moving disk at a Reynolds number of 10^5. We measure the force on the disk and the flow with PIV in a planar cross section through the center of the disk during the deceleration of the disk. It is shown that the forces are not properly predicted by the conventional Morison equation, which predicts the drag force based on the instantaneous velocity and acceleration.

BACKGROUND

The Morison equation (Morison *et al.*, 1950) is commonly used to describe the drag force $F_D(t)$ on an object in a flow with a time-dependent flow velocity $U(t)$:

$$F_D(t) = \underbrace{C_D \cdot \tfrac{1}{2}\rho U^2(t) \cdot A}_{F_{\rm QS}(t)} + F_{\rm a}(t), \qquad (1)$$

where $F_{\rm QS}(t)$ is the quasi-steady drag force, with C_D the stationary drag force coefficient, ρ the fluid density, and A the frontal area of the object, and $F_{\rm a}(t)$ is the drag force due to the acceleration of the object. When an object in a fluid is accelerated, the surrounding fluid also needs to be accelerated. The rate of change in the kinetic energy T of the surrounding fluid gives rise to an additional force F_x given by:

$$\frac{dT}{dt} = \underbrace{m_{\rm h}\frac{dU}{dt}}_{F_x} \cdot U, \quad \text{with:} \quad T = \tfrac{1}{2} m_{\rm h} U^2, \qquad (2)$$

where $U(t)$ is the velocity of the object, and $m_{\rm h}$ an equivalent mass of the fluid that is accelerated with the object. The equivalent mass $m_{\rm h}$ is commonly referred to as the hydrodynamic or ‘added mass’, which is conventionally computed using potential flow for the motion of the fluid around the accelerating object (Batchelor, 1967). The added mass, as computed from potential flow, is constant, so that the added mass force F_x is directly proportional to the acceleration of the object, i.e. $F_x = m_{\rm h}\, a(t)$, with: $a(t) = dU/dt$. We refer to this as the ‘inviscid added mass force’.

Lighthill (1986) mentions that the original expression for $F_{\rm QS}(t)$ in (1) needs to be refined to account for vortical motion, such as vortex shedding; no doubt is given to the added mass term in (1). However, recent findings show that the force $F_{\rm a}(t)$ for a thin plate that moves normal to its surface is not directly proportional to the acceleration (Grift *et al.*, 2019; Fernando *et al.*, 2020; Reijtenbagh *et al.*, 2023*a*).

For a thin flat plate that moves in the direction normal to the plate surface, the drag force coefficient C_D is constant when the Reynolds number exceeds 10^3; in other words, the quasi-steady drag force is given by the pressure drag, proportional to the stagnation pressure $\frac{1}{2}\rho U^2$ at the upstream side of the plate multiplied with the plate surface A and a proportionality constant C_D that depends on the plate geometry.

Extensive measurements reported by Reijtenbagh *et al.* (2023*a*) show that $F_{\rm a}(t)$ for accelerating plates scales proportional to the square root of the acceleration. The initial flow pattern around the accelerating plate strongly resembles that of an irrotational potential flow around a thin plate. When the plate further progresses, vorticity appears at the plate edges, and a vortex loop forms at the plate edge that gains circulation the plate steadily increases its velocity. At the same time, the acceleration drag force $F_{\rm a}(t)$ grows proportional to $\sim \sqrt{Ua}$ (Reijtenbagh *et al.*, 2023*a*), and exceeds the value of the inviscid added mass force predicted by potential flow theory. The force reaches its peak value at the end of the acceleration phase, and when the plate assumes a steady motion at a constant velocity, the drag force $F_D(t)$ relaxes to its stationary value $F_{\rm QS}$. At the end of the acceleration phase the vortex loop detaches from the plate edge, and a turbulent wake is formed (Grift *et al.*, 2019; Reijtenbagh *et al.*, 2023*a*,*b*).

These results indicate that the inviscid added mass force is not adequate in predicting the correct force on an accelerating plate. Reijtenbagh *et al.* (2023*a*) propose a history-based model to predict the force $F_{\rm a} \sim \sqrt{Ua}$, which shows the same qualitative behavior at the start and end of the acceleration phase as predicted by the inviscid added mass force. The model proposed by Reijtenbagh *et al.* (2023*a*) is based on the concept of drag on a moving body that was originally described by Burgers (1921), where vorticity is continuously generated at the surface of the object, and then ‘washed away’ by the external flow, and a new layer of vorticity is then generated at the surface; this continuous generation of vorticity is represented as the impulse of the flow. Hence, there is a debate on the validity of using potential flow theory to predict the forces on accelerating objects, and in particular thin plates.

The 1-D model proposed by Reijtenbagh *et al.* (2023*a*) to predict the unsteady drag force is defined as follows:

$$F_{\rm a} = C_a \rho A \sqrt{\nu U a}, \qquad (3)$$

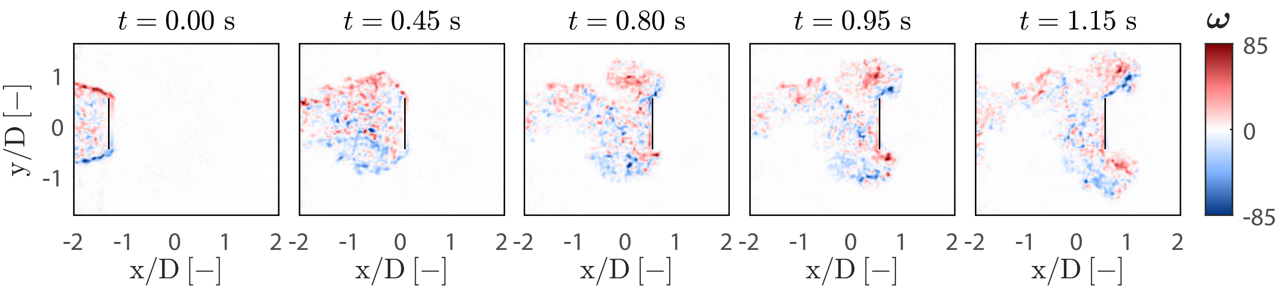

Figure 1. Five subsequent snapshots of the vorticity field during the deceleration ('A' in Figure 3) and the relaxation phase ('B' in Figure 3), corresponding to the red markers '+' in Figure 3.

where ρ and ν are the density and the kinematic viscosity of the fluid, respectively, A is the frontal area of the thin object, U is the velocity, a is the acceleration, and C_a is the instationary coefficient that depends on the geometry of the object. Replacing the added mass term by (3), the new drag force model is given by:

$$F_R(t) = \underbrace{C_D \cdot \tfrac{1}{2}\rho U^2(t) \cdot A}_{F_{\mathrm{QS}}(t)} + \underbrace{C_a \rho A \sqrt{\nu U a}}_{F_{\mathrm{a}}(t)}. \quad (4)$$

EXPERIMENTS

To test the validity of the newly proposed model, we now consider a *decelerating* round plate. We start a round plate in a large tank and let it travel a distance at constant velocity ($U_a = 0.6$ m/s) so that it has developed a stationary turbulent wake with a Reynolds number of $Re = 96\times10^3$. We then decelerate this plate at various rates and measure the force during the deceleration phase, until the plate comes to a full stop. Because the initial state before the plate starts to decelerate is clearly not irrotational, it is evident that potential flow theory and the conventional inviscid added mass cannot be applied. We use particle image velocimetry (Adrian & Westerweel, 2011) to measure the flow in a plane through the center of the round disk. The PIV result provides insight in the flow around the plate during the deceleration phase. The measurements are repeated 17 times, since the initial condition before the deceleration is turbulent, and we would like to describe the average behavior of the force on the plate during the deceleration phase.

In Figure 2 we show a schematic of the experimental setup where the round plate is traversed with given velocity and acceleration by a large gantry robot through a $5\times2\times0.6$ m^3 water-filled tank. The round plate is made of stainless steel and has a diameter of 160 mm and a thickness of 4 mm. It is connected to the gantry robot by a streamlined strut. A force transducer between the strut and the robot measures the force on the plate (and the strut), with a resolution of 31×10^{-3} N. The distance between the submerged disk and the free surface of the water is 120 mm. The PIV measurements provide information about the rate of change in kinetic energy of the flow around the plate during the deceleration phase, so that we can compute the hydrodynamic mass contribution or effective time-dependent 'added mass' $m_{\mathrm{h}}(t)$ during the deceleration. At the same time, the PIV results provide quantitative information on the generation and transport of vorticity and shear layers, and the circulation of vortices and shear layers around the decelerating object. We measure the flow in a thin laser light sheet with a thickness of about 3 mm that illuminates a planar cross section of the flow through the center of the round plate. The light beam from the pulsed laser is split in two beams that are each transformed into a light sheet that illuminates the flow from opposite directions, in order to avoid shadow regions. The PIV high-speed camera is located below the tank and observes the flow via a 45-degree mirror. The camera has a resolution of 4 MP, and a recording rate of 1 kHz. The water in the tank is seeded with fluorescent red tracer particles with diameters in the range of 75–90 μm, and density of 0.995 g/cc. The recorded images are processed using commercial software DaVis 11. The final size of the interrogation windows is 32×32 px with 75% overlap between adjacent in-

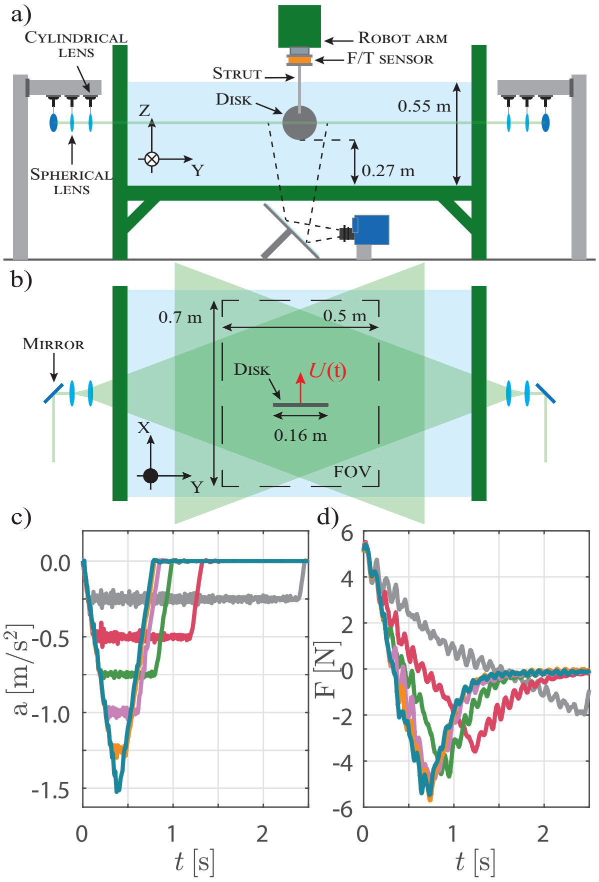

Figure 2. End view (a) and top view (b) of the experimental setup. Details are given in the text. Six different deceleration rates (c) and the corresponding drag force response (d) averaged over 17 repetitions, from steady velocity to full stop of the disk. The time instant $t = 0$ s corresponds to the start of deceleration.

terrogations, yielding a data spacing of 2.53 mm.

RESULTS

In Figure 2 c) we show the deceleration rates $a(t)$ of the motion of the disk as a function of time. The disk is first accelerated to a target velocity U_a=0.60 m/s. When it has reached the target velocity and assumes a steady velocity, the force first drops, and then rises again to assume the stationary drag force before starting the deceleration. This drop in drag force below its stationary value is due to the initial pinch-off of the vortex ring that is formed at the start of the motion (Fernando & Rival, 2016). To establish a fully developed turbulent wake that has no memory of the start-up, the disk continues to be translated for 1.7 sec. The disk is then decelerated at a rate between 0.25 and 1.50 m/s^2, with a maximum absolute jerk of 4 m/s^3. The jerk is limited to avoid erratic motion of the disk. The panel d) of Figure 2 shows the measured drag force on the disk during deceleration. The force actually changes sign, as the wake of the disk impacts the downstream side of the disk. It is already evident from these results that force does not scale proportionally to the magnitude of the deceleration.

In Figure 1 a)-e) we present the results of the PIV measurements when the disk decelerates at 0.75 m/s^2. The time instants of PIV snapshots are indicated by the red '+' symbols in Figure 3 along the drag force signal. The time instant coinciding with the start of deceleration is set as $t = 0$ s. The first snapshot (a) is taken at the moment the disk starts to slow down. The wake flow is characterized by a turbulent wake bounded by shear layers that appear to be fed by the vorticity generated by the Hiemenz flow (Emanuel, 2000) at the upstream side of the disk. The snapshots at $t = 0.45$ s and 0.80 s represent the characteristic flow field of the deceleration phase, where the wake, that now has a higher velocity than the disk, impinges on the downstream side of the disk. At $t = 0.80$ s, the wake overtakes the disk from left to right, generating a vortex pair that is clearly visible at the instant when the force reached the peak ($t = 0.95$ s). At $t \approx$1.0 s the disk has reached a full stop, but there is still a force acting on the disk, although both the velocity and the acceleration are zero. This phase is called relaxation phase (Figure 3 'B'), and demonstrates that the Morison equation in (1) is not valid, and underwrites the notion that the drag force for a decelerating plate is a history force, as described by Reijtenbagh *et al.* (2023*a*). After reaching the force peak (Figure 1 e)), the wake still impinges on the disk, pushing it from left to the right. This affects the relaxation phase of the drag force.

In Figure 3, the drag force signal is plotted as function of time, and compared to the force estimation provided by (1). As mentioned above, the force estimation based on Morison's equation underestimates the force peak, and completely misses the relaxation phase, since the effect of added mass term ceases once the plate stops accelerating. The contribution of hydrodynamic force due to the acceleration can be isolated from the measured drag: $\widetilde{F}_{\mathrm{a}} = F_D - F_{\mathrm{QS}}$, where $F_{\mathrm{QS}} = \frac{1}{2}\rho A C_D U(t)^2$. The stationary drag coefficient C_D is estimated from experimental measurements by means of average of all force signals over the steady-state phase: $C_D = \frac{\bar{F}_D}{\frac{1}{2}\rho A U_a^2}$, resulting in $C_D = 1.41$. This value is above the range of $1.14-1.17$ for drag coefficient of a disk mention in the classical literature. A comparable value was found in Fernando & Rival (2016), where the drag coefficient reached a steady-state value above 1.5 after traveling 17 diameters.

In Reijtenbagh *et al.* (2023*a*), the hydrodynamic force peak was found to scale as $\widehat{F}_{\mathrm{a}} \propto \sqrt{a}$. In this study, the same approach is used in order to verify whether the same scaling law can be used to estimate the drag force acting on a decelerating disk, even though the physics of the problem differ substantially from the case of acceleration from rest. In Figure 4 (a), the force peak of F_{a} (averaged over 17 repetitions) is plotted against the deceleration rate. Despite the deviation caused by the turbulent wake and highlighted by the error bars, the mean value follows the curve described by (3), where the empirical value of the coefficient C_a for a round plate with diameter of 159.6 mm is $C_a = 311$. In Figure 4 (b), the measured drag force F_D for $a = 0.25-1.00$ m/s^2 is compared with the estimation resulting from (4), which follows the trend of the measurements. The force peak is reproduced with good accuracy.

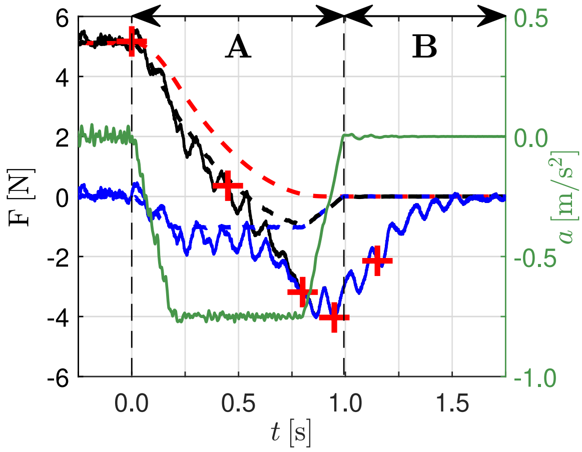

Figure 3. The black solid line is the measured drag force F_D. The green solid line is the deceleration output of the robot, $a(t)$. The red dashed line is the quasi-steady force: $F_{\mathrm{QS}}(t) = \frac{1}{2}\rho A C_D U(t)^2$, while the blue solid line represents the hydrodynamic force due to the acceleration: $\widetilde{F}_a = F_D - F_{\mathrm{QS}}$. The blue dashed line is added mass term: $F_x = m_{\mathrm{h}} a(t)$, where $m_{\mathrm{h}} = \frac{8}{3}\rho r^3$ is the added mass for a infinitely thin disk, derived from potential theory. The black dashed line is the total force estimate by means of Morison's equation (Morison *et al.*, 1950): $F_{\mathrm{M}} = F_{\mathrm{QS}} + F_x$. 'A' and 'B' specify the deceleration and the relaxation phase, respectively.

CONCLUSIONS

In this study, the force response acting on decelerating thin disk, that moves normal to the flow, is investigated. The presence of a fully turbulent wake when the plate starts to decelerate makes evident that potential flow theory cannot be applied to estimate the drag force acting on the object. Instead, the model proposed by Reijtenbagh *et al.* (2023*a*) shows a reasonable good agreement with the measured drag force during the deceleration phase, despite the severe effects of the wake. In fact, this latter moves faster than the disk and apply a thrust in the opposite direction of the drag force, as clearly visible from PIV snapshots in Figure 1. This seems to be the cause of the deviation observed in the force measurements, and highlighted in Figure 4 (a).

Future analysis will focus on the effects of the wake. Moreover, special attention will be dedicated to the impact of the constant jerk phase, during which the acceleration increases linearly, for example cases $a = 1.25$ and 1.5 m/s^2 (see Figure 2 (c)). In fact, the 1-D model used to estimate the force

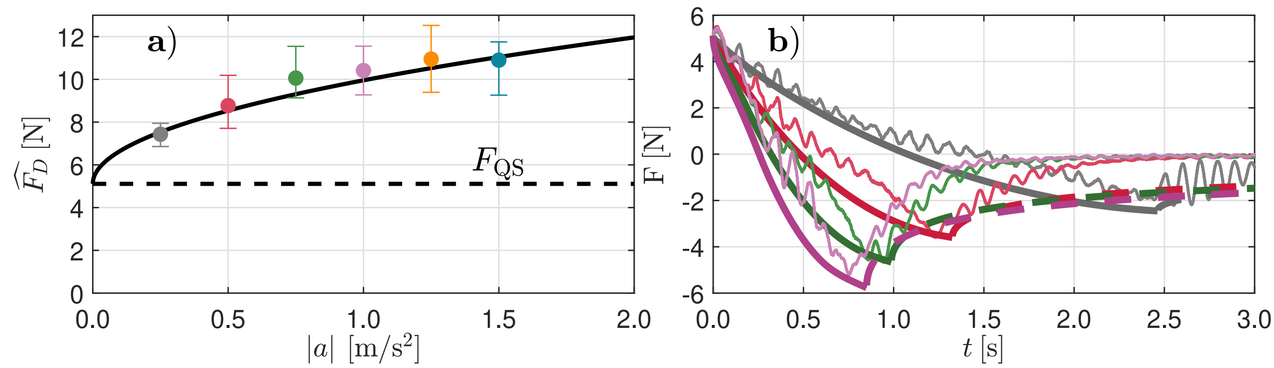

Figure 4. In panel a) the force peak of $\widetilde{F_a}$ as function of the acceleration (absolute value). The force peak is averaged over 17 repetitions. The error bars represents the minimum and the maximum values. The black solid line is the curve outlined by $C_a \rho A \sqrt{\nu U_a}\sqrt{a}$, while the black dashed line is the quasi-steady force: $F_{QS}(t) = \frac{1}{2}\rho A C_D U_a^2$. In panel b), the measured drag force $F_D(t)$ (thin solid line) is compared with the force estimation (thick solid line, in darker colors) $F_R(t)$ (4). The colors correspond to those used for the corresponding deceleration rate in panel a).

is meant to work with a constant acceleration of the object. Finally, the relaxation phase of the model (dashed line in Figure 4 (b)) needs to include the wake effect, since the decay does not follow the measured one, which decays faster.

REFERENCES

Adrian, R. J. & Westerweel, J. 2011 *Particle Image Velocimetry*. Cambridge University Press.

Batchelor, G. K. 1967 *An Introduction to Fluid Mechanics*. Cambridge University Press.

Burgers, J. M. 1921 On the resistance of fluids and vortex motion. *Proc. K. Ned. Akad. Wet.* **23**, 774–782.

Emanuel, G. 2000 *Analytical Fluid Dynamics*, 2nd edn. CRC Press.

Fernando, J. N. & Rival, D. E. 2016 Reynolds-number scaling of vortex pinch-off on low-aspect-ratio propulsors. *J. Fluid Mech.* **799**, R3.

Fernando, J. N., Weymouth, G. D. & Rival, D. E. 2020 On the limits of added-mass theory in separated flows and with varying initial conditions. *J. Fluid. Struct.* **93**, 102835.

Grift, E. J., Vijayaragavan, N. B., Tummers, M. J. & Westerweel, J. 2019 Drag force on an accelerating submerged plate. *J. Fluid Mech.* **866**, 369–398.

Lighthill, J. 1986 Fundamentals concerning wave loading on offshore structures. *J. Fluid Mech.* **173**, 667–681.

Morison, J. R., O'Brien, M. P., Johnson, J. W. & Schaaf, S. A. 1950 The force exerted by surface waves on piles. *J. Petrol. Technol.* **2**, 149–154.

Reijtenbagh, J., Tummers, M. J. & Westerweel, J. 2023*a* Drag force on a starting plate scales with the square root of acceleration. *Phys. Rev. Lett.* **130**, 174001.

Reijtenbagh, J., Westerweel, J. & van de Water, W. 2023*b* Transition to turbulence behind a traveling plate. *Phys. Rev. Fluids* **8**, 104601.